

Effect of plasma composition on magnetized outflows

Kuldeep Singh^{1,2}, Indranil Chattopadhyay^{1*}

¹*Aryabhata Research Institute of Observational Sciences (ARIES), Manora Peak, Nainital-263002, India.*

²*University of Delhi, Delhi, India.*

ABSTRACT

In this paper, we study magnetized winds described by variable adiabatic index equation of state in Paczyński & Wiita pseudo-Newtonian potential. We identify the flow solutions with the parameter space of the flow. We also confirm that the physical wind solution is the one which passes through the slow, Alfvén and fast critical points. We study the dependence of the wind solution on the Bernoulli parameter E and the total angular momentum L . The adiabatic index, which is a function of temperature and composition, was found to be variable in all the outflow solutions. For the same values of the Bernoulli parameter and the total angular momentum, a wind in strong gravity is more accelerated, compared to a wind in Newtonian gravity. We show that flow variables like the radial and azimuthal velocity components, temperature all depend on the composition of the flow. Unlike the outflow solutions in hydrodynamic regime, the terminal speed of a magnetically driven wind also depends on the composition parameter.

Key words: Magneto hydrodynamics (MHD); Outflows; Stars: Neutron stars; Black Hole

1 INTRODUCTION

There are many magneto-hydrodynamic (MHD) studies of winds around central gravitating objects. For example, Mestel (1967, 1968) studied loss of angular momentum and magnetic breaking and Weber & Davis (1967, hereafter WD) studied the solar wind by solving MHD equations self-consistently. Their model is well tested and predicted the wind speed at the earth’s orbit. Studies of winds were further carried out by Pneuman (1971); Okamoto (1974,

* Email: kuldeep@aries.res.in (KS); indra@aries.res.in (IC)

1975). Later Sakurai (1985, 1987) generalized WD wind model and studied wind away from the equatorial plane and its collimation by the magnetic field. The generalization of magnetized winds later became the starting point of studies on magnetically driven jets (Camenzind 1986; Lovelace et. al. 1991, 1995; Daigne & Drenkhahn 2002; Polko et. al. 2010). It may be noted that, Blandford & Payne (1982) studied accretion disc particles being flung along the poloidal magnetic field lines, the foot points of which are co-rotating with the Keplerian accretion disc. This model is similar to a bead on a wire scenario. The assumption of cold flow limits the solutions to a trans-Alfvénic and trans-fast flow and therefore, these solutions are oblivious of the location of slow-magnetosonic points. Moreover, one may note, Keplerian disc may not be the base of the jet but the corona (or, the hotter, inner part of the accretion disc) might actually be the base. Therefore, studying hot flow near the compact object is quite important.

The outflow models which did consider hot flow (for e. g., Camenzind 1986; Lovelace et. al. 1991), the authors have used constant adiabatic index (Γ) equation of state (EoS) to describe the thermodynamics of the plasma. However, if we implement any of these models at regions around compact objects (hot stars, neutron stars, black holes), which are hotter than the environ of ordinary stars, then fixed Γ EoS is not valid. In other words, close to the central object, the flow should be hot enough such that $\Gamma \gtrsim 4/3$, but at asymptotically large distances $\Gamma \sim 5/3$, which is equivalent to temperature variation of more than four orders of magnitude. Such temperature variation is expected in outflows. In this paper, instead of focusing on jets, we concentrate on the role that correct plasma thermodynamics may play on the WD type wind solutions. We consider a variable Γ equation of state (abbreviated as CR EoS, Chattopadhyay & Ryu 2009) and obtain outflow solutions for winds around compact objects. We use Paczyński & Wiita (PW) potential (Paczyński & Wiita 1980) to study the behaviour around a stronger gravity. However, we would like to understand the role which strong gravity might play on such wind solutions by comparing with the winds in Newtonian potential.

One of the advantage of using CR EoS is that, this EoS has composition parameter ξ , therefore we can also study effect of composition on wind solution in the present manuscript. The composition of the flow, controls the inertial and thermal energy budget of the outflow. It may be noted that, the effect of composition has been studied (by employing CR EoS) in outflows and jets (Vyas et. al. 2015; Vyas & Chattopadhyay 2017, 2018, 2019), as well as, in accretion (Kumar et al. 2013; Kumar & Chattopadhyay 2014; Chattopadhyay & Kumar

2016; Kumar & Chattopadhyay 2017), but all in the realm of hydrodynamic regime. CR EoS has been employed for magnetized accretion onto neutron stars (Singh & Chattopadhyay 2018), but assumption of strong magnetic field simplified the equations of motion immensely such that the flow remained sub-Alfvénic. Therefore, this will probably be the first study where the issue of composition can be systematically addressed for flows in the proper MHD scenario. In this paper, we would like to investigate the entire parameter space for various flow parameters including the composition parameter of the flow. We would also like to investigate how the actual flow solution is affected by the composition of the flow. We intend to investigate many such questions in this paper.

The present manuscript is arranged in the following way. In the section 2.1, we present ideal magneto-hydrodynamic (MHD) equations. In the section 2.2, we discuss the relativistic equation of state (EoS) having temperature dependent adiabatic index. In the section 3, we explain the methodology to solve the equations of motion. In the section 4, we present the parameter space for the critical points and outflow/wind solutions. Finally in section 5 we present discussions and the concluding remarks.

2 MHD EQUATIONS AND ASSUMPTIONS

2.1 Governing equations

We assume that the flow is steady, inviscid and a highly conducting plasma. Therefore, MHD equations have the following form (Weber & Davis 1967; Heinemann & Olbert 1978),

$$\nabla \cdot (\rho \mathbf{v}) = 0, \quad (1)$$

$$\nabla \cdot \mathbf{B} = 0, \quad (2)$$

$$\nabla \times (\mathbf{v} \times \mathbf{B}) = 0, \quad (3)$$

$$(\rho \mathbf{v} \cdot \nabla) \mathbf{v} = -\nabla p + \frac{1}{c} (\mathbf{J} \times \mathbf{B}) - \Phi'(r) \hat{\mathbf{r}} \quad (4)$$

Here, $\Phi(r)$ is the gravitational potential and $\Phi(r) = \Phi_{\text{NP}}(r) = -GM/r$, is the Newtonian potential and its derivative is $\Phi'(r) = \Phi'_{\text{NP}}(r) = GM/r^2$. The PW potential $\Phi(r) = \Phi_{\text{PWP}}(r) = -GM/(r - r_g)$ and its derivative is $\Phi'(r) = \Phi'_{\text{PWP}}(r) = GM/(r - r_g)^2$ where the Schwarzschild radius is $r_g = 2GM/c^2$, G is the gravitational constant and M is the mass of the central object and c is the speed of light in vacuum. Assuming ideal MHD, we integrate MHD equations along magnetic field lines and axis symmetry assumption to obtain the con-

served quantities as:

(i) The mass flux conservation is obtained from the continuity equation (1),

$$\rho v_r r^2 = \text{constant} = \dot{M}, \quad (5)$$

(ii) The magnetic flux conservation is obtained from the Maxwell's equation (2),

$$B_r r^2 = \text{constant} = B_o r_o^2, \quad (6)$$

(iii) The Faraday equation (3), for highly conducting fluid gives,

$$r(v_r B_\phi - v_\phi B_r) = \text{constant} = -\Omega B_r r^2, \quad (7)$$

(iv) r^{th} component of momentum balance equation (4) gives the total energy conservation,

$$\frac{1}{2}v_r^2 + \frac{1}{2}v_\phi^2 + h + \Phi(r) - \frac{B_\phi B_r \Omega r}{4\pi\rho v_r} = \text{constant} = E, \quad (8)$$

(v) ϕ^{th} component of momentum balance equation (4) gives the total angular momentum conservation,

$$r v_\phi - \frac{B_\phi B_r r}{4\pi\rho v_r} = \text{constant} = L. \quad (9)$$

Here r is the radial distance, r_o is the radius of a star, or, the radial distance near black hole, ρ is the mass density, v_r is the radial velocity component, v_ϕ is the azimuthal velocity component, B_r is the radial magnetic field and subscript 'o' denote the magnetic field at distance r_o , B_ϕ is the azimuthal magnetic field, Ω is the angular velocity of star or matter at r_o . In equation (9), we see that total angular momentum has two terms, the first term is the angular momentum associated with matter and the second term represents the angular momentum associated with the magnetic field. Therefore, only sum of both angular momenta is conserved and not the individual entities. This also imply that angular momentum can be exchanged between matter and field. The radial Alfvénic Mach number is defined by

$$M_A^2 = \frac{4\pi\rho v_r^2}{B_r^2}, \quad (10)$$

From equations (7) and (9), we can derive the expression for v_ϕ ,

$$v_\phi = \Omega r \frac{(M_A^2 L r^{-2} \Omega^{-1} - 1)}{(M_A^2 - 1)}. \quad (11)$$

2.2 Variable Γ EoS

So far we have discussed that adiabatic index does not remain constant throughout the flow. Chandrasekhar (1938) obtained the exact EoS of hot gas which has a variable adiabatic index. But it is difficult to use this EoS in numerical calculations due to the presence of modified Bessel functions of second kind, which we know has a non terminating form.

However, there is another approximate but accurate EoS (compared to Chandrasekhar EoS) given by Chattopadhyay & Ryu (2009) for multi-species flow (*i.e.*, composed of electron, positron and proton) having variable adiabatic index — the CR EoS. In our analysis, we use CR EoS, because it has a simple functional form $f(\Theta, \xi)$ instead of complicated Bessel functions. The energy density (\bar{e}) is given by,

$$\bar{e} = \frac{\rho c^2 f(\Theta, \xi)}{K}; \text{ where,} \quad (12)$$

$$f(\Theta, \xi) = (2 - \xi) \left[1 + \Theta \frac{(9\Theta + 3)}{(3\Theta + 2)} \right] + \xi \left[\frac{1}{\eta} + \Theta \frac{(9\Theta + 3/\eta)}{(3\Theta + 2/\eta)} \right].$$

The $\Theta = \kappa_B T / (m_e c^2)$ is proportional to T , $\rho = n_{e^-} m_e K$ is the total rest-mass density, $\eta = m_{e^-} / m_p$ is electron to proton mass ratio and $\xi = n_p / n_{e^-}$ is the composition parameter which is the ratio of number density of protons to the number density of electrons. The constant $K = [2 - \xi(1 - 1/\eta)]$ depends on the composition of the flow. A plasma described by $\xi = 0.0$ has no protons and therefore is an electron-positron plasma, for $0.0 < \xi < 1.0$ we have electron-positron-proton plasma and $\xi = 1.0$ signify electron-proton plasma. It may be noted that, $\xi = 0.0$ plasma is unlikely to exist as a global solution *i. e.*, spanning from a region close to the compact object to asymptotically large distance. As a result, no such solution has been presented in the results section (4). We expect the composition of the outflow to be electron-proton, however for flows which start with very high temperature or in intense high energy radiation region (near black hole or neutron star) may have significant electron-positron pairs in the flow, so pair dominated plasma (with some protons) is quite possible. Since composition of outflows have not been conclusively established in observations, therefore in this paper, we have studied how composition of the plasma may affect the outflow solutions by using ξ as a parameter in the range $0 < \xi \leq 1$. However, to predict an observational signature of composition would require detailed radiative processes of magnetized plasma, which is beyond the scope of the present work.

Enthalpy (h), variable adiabatic index (Γ), polytropic index N and sound speed (c_s) are given by,

$$h = \frac{\bar{e} + p}{\rho} = \frac{f c^2}{K} + \frac{2\Theta c^2}{K} \quad (13)$$

and

$$\Gamma = 1 + \frac{1}{N}, \quad N = \frac{1}{2} \frac{df}{d\Theta} \text{ and } c_s^2 = \frac{2\Theta \Gamma c^2}{K}. \quad (14)$$

The adiabatic equation of state can be obtained by integrating the 1st law of thermodynamics with the help of the continuity equation and CR EoS (Kumar et al. 2013; Vyas et. al. 2015;

Singh & Chattopadhyay 2018), to obtain

$$\rho = \mathcal{Q} \exp(k_3) \Theta^{3/2} (3\Theta + 2)^{k_1} (3\Theta + 2/\eta)^{k_2}, \quad (15)$$

where, $k_1 = 3(2 - \xi)/4$, $k_2 = 3\xi/4$ and $k_3 = (f - K)/(2\Theta)$ and \mathcal{Q} is the measure of the entropy. Using equation (5), the entropy-accretion rate \dot{M} is given by,

$$\dot{M} = \frac{\dot{M}}{4\pi\mathcal{Q}} = v_r r^2 \exp(k_3) \Theta^{3/2} (3\Theta + 2)^{k_1} (3\Theta + 2/\eta)^{k_2} \quad (16)$$

One may note that, \dot{M} is a temperature and composition dependent measure of entropy, which remains constant along a non-dissipative flow, or in absence of shocks.

3 METHODOLOGY

We know that plasma has three signal speeds *i.e.*, slow speed (u_S), Alfvén speed (in our case we are using radial Alfvén speed u_A) and fast speed (u_F). In the present case, the order of these speeds are $u_S < u_A < u_F$. We know that for outflows, radial velocity (v_r) is very small near the surface of star or a radius near the black hole, therefore, $M_A \ll 1$ and very far from the central object, $M_A \gg 1$. Therefore, at certain radius (say r_A), v_r is equal to u_A (*i.e.*, $v_r|_{r_A} \equiv v_{Ar} = u_A$) but at that radius, denominator of v_ϕ is zero (see equation 11). Thus the numerator should also be zero at that critical radius to make v_ϕ always finite and this point is known as Alfvénic critical point. Therefore, numerator of v_ϕ gives a relation between the critical radius of the Alfvénic point and total angular momentum,

$$L = \Omega r_A^2. \quad (17)$$

Using equations (5), (6) and (10), we can also write M_A^2 as,

$$M_A^2 = \frac{v_r r^2}{v_{Ar} r_A^2} = \frac{\rho_A}{\rho}. \quad (18)$$

and v_ϕ and B_ϕ become,

$$v_\phi = \frac{\Omega r}{v_{Ar}} \left(\frac{v_{Ar} - v_r}{1 - M_A^2} \right) \quad \text{and} \quad B_\phi = -B_r \frac{\Omega r}{v_{Ar} r_A^2} \left(\frac{r_A^2 - r^2}{1 - M_A^2} \right). \quad (19)$$

The r^{th} -component of momentum balance equation (4) gives the equation of motion,

$$\frac{dv_r}{dr} = \frac{\mathcal{N}}{\mathcal{D}}, \quad (20)$$

$$\mathcal{N} = v_r r \left\{ \left(\frac{2c_s^2}{r^2} - \frac{\Phi'(r)}{r} \right) (M_A^2 - 1)^3 + \Omega^2 \left(\frac{v_r}{v_{Ar}} - 1 \right) \left[(M_A^2 + 1) \frac{v_r}{v_{Ar}} - 3M_A^2 + 1 \right] \right\}$$

$$\mathcal{D} = (v_r^2 - c_s^2) (M_A^2 - 1)^3 - \frac{\Omega^2}{r^2} M_A^4 (r^2 - r_A^2)^2.$$

To find wind solution, we need two input parameters *i.e.*, E , L , initial boundary conditions and composition of flow ξ which is a free parameter. In our case, we use Alfvén point r_A

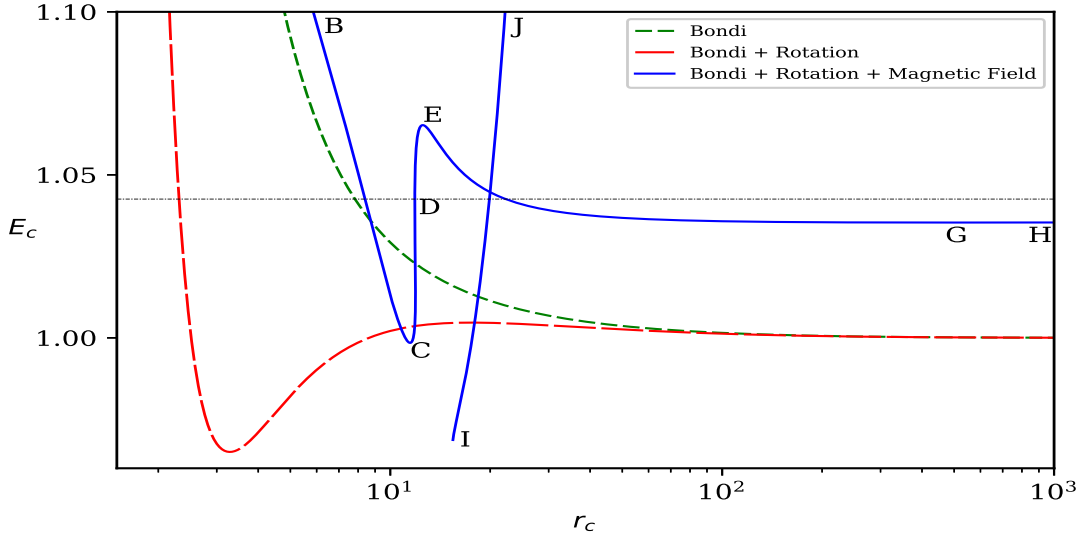


Figure 1. In this plot, total energy (E_c) is plotted versus critical radius (r_c) for Bondi flow (dashed-green), Bondi flow with rotation (long-dashed-red) and magnetized, rotating flow (solid-blue) for $L = 1.75$. Thin dashed line represent $E=1.04257$.

as the initial condition because at that radius, equation(20) or $dv_r/dr \rightarrow 0/0$. Thus, equating the numerator and denominator to zero, provides us with the critical point conditions and hence acts as mathematical boundary conditions. However, $dv_r/dr \rightarrow 0/0$ at other critical points when $v_r = u_S$ or $v_r = u_F$. These critical points are known as the slow critical point (r_S) or the fast critical point (r_F), respectively. Therefore, $\mathcal{N} = 0$ and $\mathcal{D} = 0$ are the critical point conditions to find all the critical points (slow points, Alfvén points, fast points and all of which can either be X-type or O-type) for a given set of input parameters. We have found that for a small energy range and given angular momentum, there exists possibility of five critical points. By supplying L , r_A and v_{Ar} , from the critical point conditions we can find out critical radius (r_c) and critical radial velocity v_{rc} . Then, the total energy $E = E_c$ at the critical point can be calculated from equation (8) and entropy accretion rate ($\dot{\mathcal{M}} = \dot{\mathcal{M}}_c$) from equation (16). With the help of L'Hospital rule, we determine the gradient of v_r at the critical points. We integrate the equation of motion forward and backward from the critical points with the help of 4th order Runge-Kutta method and find the complete wind solution.

4 RESULTS

In this paper, the unit of velocity is the speed of light c in vacuum and that of distance is the Schwarzschild radius r_g . We have used Alfvén point as initial conditions, so we have chosen $r_A = 11.85$ and $v_{Ar} = 0.167$ for Fig.(1), where we have plotted Bernoulli parameter or

specific energy (E_c) at the critical point versus the critical radius (r_c) for Bondi flow (dashed, green), Bondi flow with rotation (long-dashed, red) and Bondi flow with both the rotation and magnetic field (solid, blue) for total angular momentum $L = 1.75$ and $\xi = 1$ where strong gravity is mimicked by PW potential. Purely Bondi flow (i. e., hydrodynamic flow and only radial velocity component) harbours a single critical point (a sonic point where $v_r = c_s$) for any value of r_c , which is clear from the dashed (green) curve, which is a monotonically decreasing function of r . It may be noted, that the sonic or critical point occurs in a fluid, due to the presence of gravity. A sufficiently hot gas confined very close to the central object would expand against gravity. However, due to $\sim (r - r_g)^{-2}$ nature of gravity, it will fall faster than the thermal term ($2c_s^2/r$). Since the kinetic term gains at the expense of both gravity and thermal term, at some point $v_r \geq c_s$, i. e, the flow becomes transonic at the critical point. The E_c — r_c curve (dashed, green) is a monotonically decreasing function, and therefore, for any given $E = E_c$ the Bondi flow admits only one sonic point.

However, for a Bondi-rotating flow (hydrodynamic, v_r and v_ϕ components), the effective gravity deviates from its usual $\sim (r - r_g)^{-2}$ form due to the presence of the centrifugal term v_ϕ^2/r . This interplay of rotation and gravity produces multiple sonic/critical points, which is also clear from the E_c — r_c curve (long-dashed, red)) which has a maximum and minimum for a given value of L . Therefore, for any value of $E = E_c$ within the two extrema, the flow would harbour multiple critical points.

Hydrodynamics is relatively simple, since in this regime there is only one signal speed i. e., the sound speed (c_s) which is basically the propagating pressure perturbations and are isotropic in nature. Magnetized flow (solid-blue) is entirely a different ball game. As has been mentioned above, there are three signal speeds in a magnetized plasma *i.e.*, slow speed, Alfvén speed and fast speed. It may be noted that propagation of the perturbations of the magnetic field is the Alfvén wave, but the competition between magnetic and plasma pressure gives rise to the slow and fast magnetosonic waves. When the plasma pressure and magnetic pressure works in phase, it is fast wave, if not then it is slow. This is precisely the reason we have three signal speed in a magnetized plasma. Even the nature of these three waves are different, Alfvén is a transverse wave, while fast and slow waves are longitudinal. Moreover, while Alfvén and slow waves are not isotropic, but fast wave is quasi-isotropic. Hence, instead of sonic points ($v_r = c_s$) as we find in hydrodynamic regime, for magnetized plasma we have slow ($v_r = u_S$) and fast ($v_r = u_F$) magnetosonic points, and Alfvén point ($v_r = u_A$).

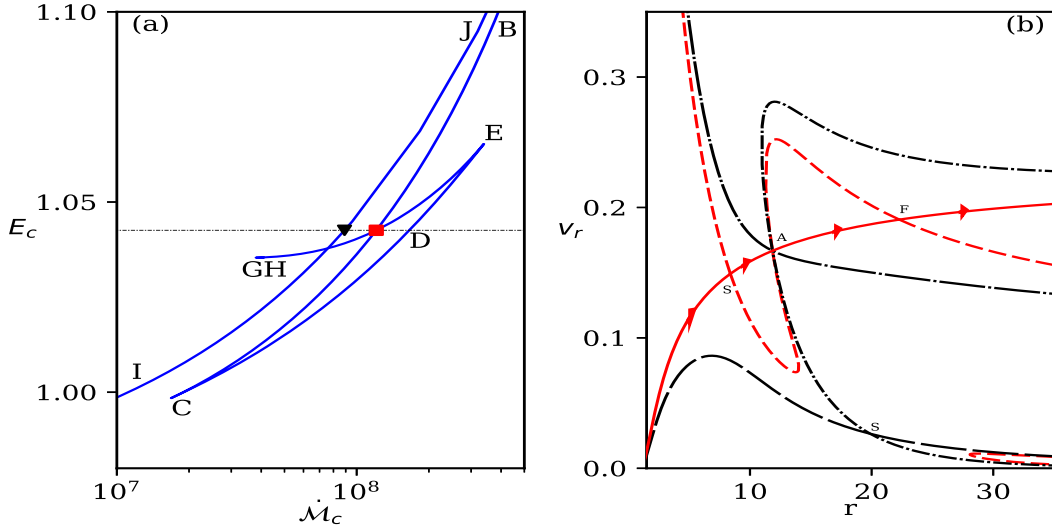


Figure 2. (a) E_c — \dot{M}_c plot corresponding to Fig. (1). The branches named BC, CD etc up to IJ are also marked on the curve. The square (red) corresponds to the outflow solution passing through slow, Alfvén and fast points. The triangle (black) represent solutions which is not passing through all three critical points. (b) v_r versus r or actual outflow solutions. The solid (red) curve with arrow heads represent the transonic wind solution passing through slow, Alfvén and fast points, marked as S, A, F, respectively. The dashed (red) curves are the transonic outflow solutions with wrong boundary condition. Long dashed curve (black) is a trans-slow solution. Dashed-dotted curve is the trans-slow, trans-Alfvén solutions and long-dashed-dotted curve is a trans-Alfvénic flow. $E = 1.04257$ (dotted, horizontal line), $L = 1.75$ for all the curves.

Above, we have discussed that multiple critical points may arise in non-magnetized plasma because of the presence of angular momentum. This also applies in magnetized plasma too. However, the additional feature is the plasma angular momentum is itself modified by the magnetic field (equation 9), therefore the effective gravity is modified by the plasma angular momentum as well as the magnetic field components. In other words, addition of rotation in magnetized plasma leads to the existence of one to four critical points in general, but within a small energy range (E_c) we have found five critical points. It means the flow can either be super-slow ($v_r > u_S$) and/or super-Alfvén ($v_r > u_A$) and/or super-fast ($v_r > u_F$) or we can say that flow can pass through one critical point or through multiple critical points similar to WD wind solution (Weber & Davis 1967). Curve marked BC represent X-type slow points, CD represent O-type slow points, DE are O-type fast points. Points on the curve EG are X-type fast points, while GH curve are O-type fast points. Curve IJ is another set of X-type slow points. The thin, dashed line is for $E = 1.04257$, which represents the outflow solution in the next figure, passes through slow, Alfvén, and fast points, or is equivalent to the classical WD solution.

In Fig. (2a), we plot the E_c with \dot{M}_c corresponding to the curves of Fig. (1). The zones marked BC, CD, DE, EG, and GH are shown on this figure too. The parameters

corresponding to the solid box (red) corresponds to the outflow solution which passes through the slow, Alfvén and fast points (i. e., the outflow is trans-slow, trans-Alfvén, trans-fast). Figure (2a) clearly shows that, wind represented by the solid box (red), possesses the same entropy ($\dot{\mathcal{M}}_c$) and energy E_c in all the three critical points. The solid inverted triangle represents a flow which has the same specific energy and total angular momentum as the flow represented by the solid box, but passes only through the slow and/or Alfvén critical points and has lower entropy. One may remember, that to find the solutions, we have to supply r_A along with E , L and ξ , and obtain the value of v_{Ar} by iteration. We choose $r_A = 11.85$ for all the solutions in this paper, till mentioned otherwise. In Fig. (2b), we plot the actual outflow solutions, corresponding to the parameters of the solid square of Fig. (2a). It may be noted $v_{Ar} = 0.167$ in this case. The solid (red) curve with arrows shows the outflow solution passing through the slow (trans-slow), Alfvén (trans-Alfvén) and fast points (trans-fast) represented on the figure as S (i. e., r_S), A (i. e., r_A), and F (i. e., r_F), respectively. This solution passes through all the critical points and is a global solution (connecting outflows near the compact object with asymptotically large distance). Since the entropy of the all the critical points are same (solid square in Fig. 2a), the wind solution is smooth. Among all possible global solutions, the one passing through S, A and F has higher entropy and therefore is the correct physical solution. This is equivalent to the WD class of solutions. The dashed curve represents the solution which also passes through S, A and F points but with boundary conditions which are opposite to that of the outflow solution and is multi-valued in a limited range of r . The boundary condition of an outflow is that it has to be sub-slow (i.e., $v_r \sim$ small) near the central object and super-fast (i.e., $v_r \sim$ high) at asymptotically large distances, which is evidently not the case for the dashed (red) curve. Other solutions which are not marked with arrows, also do not satisfy the boundary conditions of an outflow. These solutions either pass through A (long-dashed-dotted), or through A and S (dashed-dot), or at times only through S (long dashed). It is interesting to inquire about solutions for $E > 1.04257$ mark (above dotted horizontal line in Fig. 2a). Such solutions may have entropy higher than that corresponding to the solid square, but unfortunately, those solutions do not pass simultaneously through r_S , r_A , & r_F . Moreover, if there exist a global solution for such parameters, still we cannot consider them as proper solutions because those are decelerating. The resulting terminal speed therefore, is less than the solution represented by solid curve with arrows in Fig. (2b). In other words, the outflow solution for any set of $E-L$, which passes simultaneously through r_S , r_A and r_F (one with

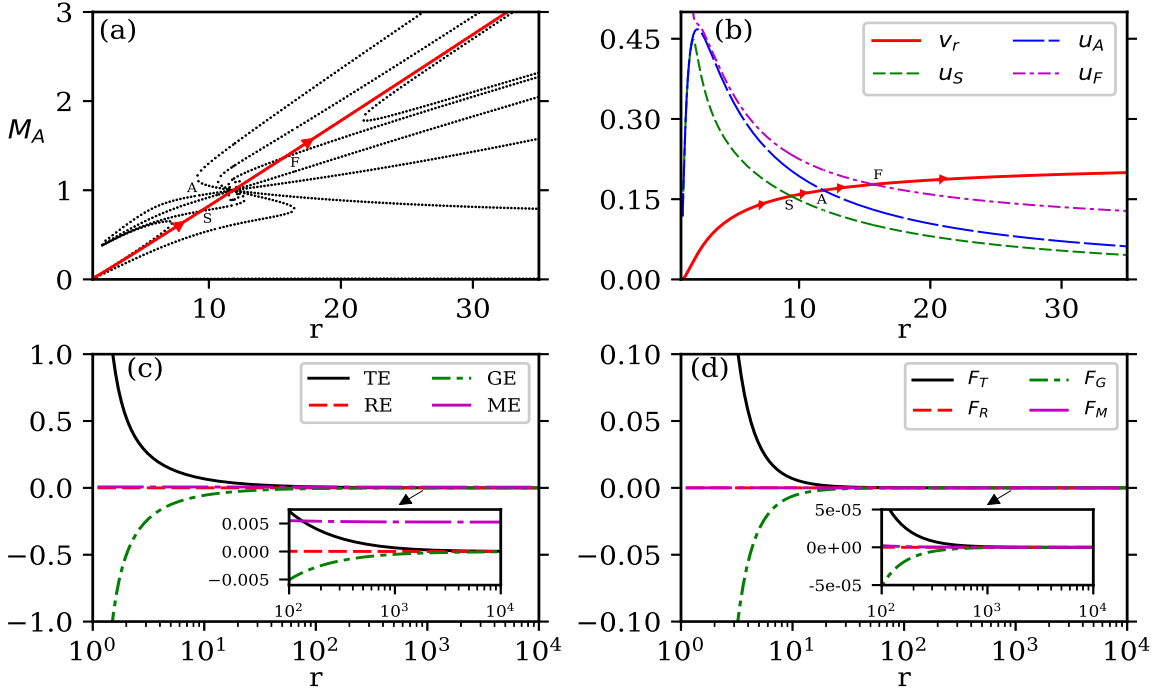


Figure 3. (a) M_A vs r as a function of r . The solid curve with arrow heads is the physical wind solution and the dotted are other unphysical branches. Location of the slow magneto-sonic, Alfvén and fast magneto-sonic points are marked as S, A and F, respectively. (b) Comparing v_r (solid with arrows, red), u_S (dashed, green), u_A (long-dashed, blue) and u_F (dashed-dot, violet) of the physical wind branch as a function of r . The locations where v_r crosses u_S , u_A and u_F are marked as S, A and F. (c) Thermal (solid, black), rotational (dashed, red), gravitational (dashed-dot, green) and magnetic (long-dashed-dotted, violet) terms of the Bernoulli parameter E are named as TE, RE, GE and ME, respectively. (d) Comparison of forces F_T (solid, black), F_R (dashed, red), F_G (dashed-dot, green), F_M (long-dashed, violet) as function of r . Panels (b–d) presents variables corresponding to the solution (solid) in panel a. The wind is for $E = 1.03075$ and $L = 1.0$. Here $\xi = 1$.

arrows) is the correct and accelerating class of wind solutions and was first pointed out by Weber & Davis (1967).

In Fig. (3a), we plot the Alfvén Mach number M_A (equation 10) as a function of r , corresponding to the physical solution (trans-slow, trans-Alfvén, trans-fast) represented as solid curve, marked with arrows. Physical wind solution passes simultaneously through all the three critical points S, A and F. The dotted curves represent other unphysical solutions. It may be noted that, ordinary Mach number distribution (i. e., v_r/c_s) is not presented in the figure. This is simply because in a magnetized plasma, sound speed works in tandem with magnetic pressure and by itself is not vitally important. However, Alfvén speed determines the flow structure, therefore, the information whether a flow is super or sub Alfvénic is important. In Fig. (3b), we compare v_r (solid with arrows, red), u_S (dashed, green), u_A (long-dashed, blue) and u_F (dashed-dot, violet) of the physical wind solution presented in the previous panel, as a function of r . These solutions corresponds to $E = 1.03075$, $L = 1.0$ and $\xi = 1$. The locations of r_S , r_A and r_F (marked as S, A and F in the figure) corresponds

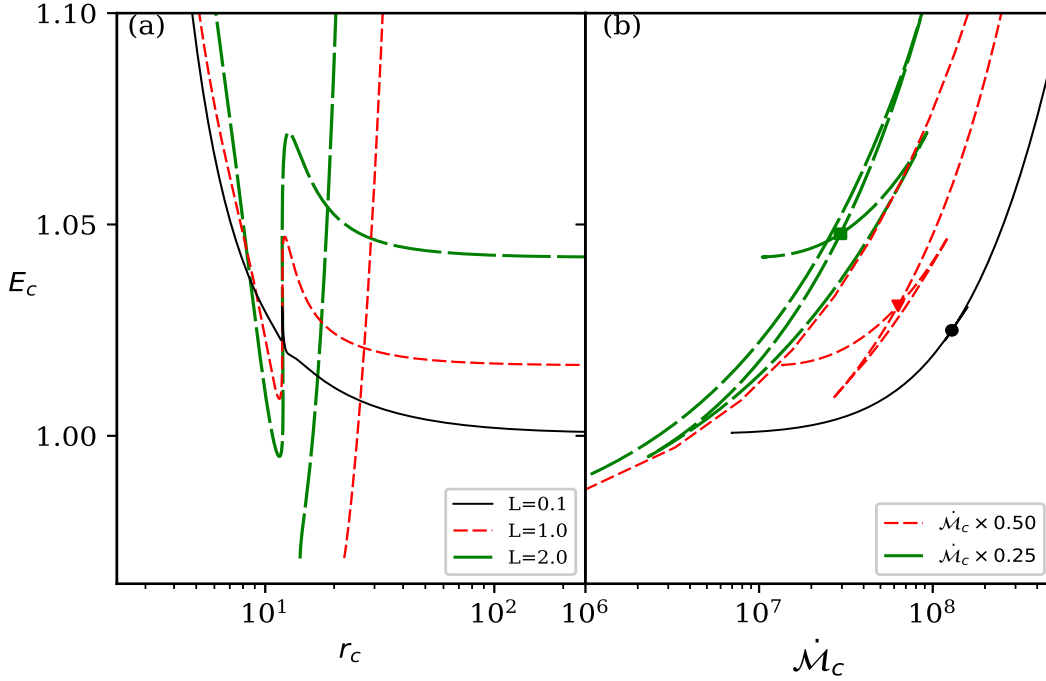


Figure 4. (a) We have plotted the total energy E_c at critical point r_c for total angular momentum $L = 0.1$ (solid, black), 1.0 (dashed, red) and 2.0 (long-dashed, green). (b) $E_c - \dot{M}_c$ for various values of $L = 0.1$ (solid, black), 1.0 (dashed, red) and 2.0 (long-dashed, green). Here $\xi = 1$.

to the intersection of v_r with u_S , u_A and u_F . In Fig. (3c), we plot various components of E , namely, the thermal or TE ($\equiv h - 1$), the rotational or RE ($\equiv v_\phi^2/2$), the gravitational or GE ($\equiv \Phi$) and the magnetic or ME ($\equiv -\{B_\phi B_r \Omega r\} / \{4\pi \rho v_r\}$) terms of equation 8. The inset zooms all the curves for $r \rightarrow$ large. Near the compact object, TE term dominates, while at $r \gtrsim 100r_g$ the ME term dominates. Similarly, we plot various force terms F_T (thermal), F_R (rotational), F_G (gravitational) and F_M (magnetic), along the streamline in Fig. 3d. Near the central object, F_T drives the flow against gravity. At large distance all the forces become comparable to each other, therefore comparing the combination of forces which competes with each other gives a better picture. The thermal force is the primary agency which opposes gravity, while magnetic force reduces v_ϕ . So we paired the competing forces like F_T and F_G and compared with the other combination F_R and F_M . At large distance the magnetic and the centrifugal forces together exceeds the thermal and the gravitational forces and drives the wind outward (see Fig. A1 in Appendix A).

We study the effect of L on outflow solutions. In Fig. (4a) we plot E_c as a function of r_c , each curve is for $L = 0.1$ (solid, black), 1.0 (dashed, red) and 2.0 (long-dashed, green). With the increase of L , the flow becomes more energetic at a given critical point. In Fig.

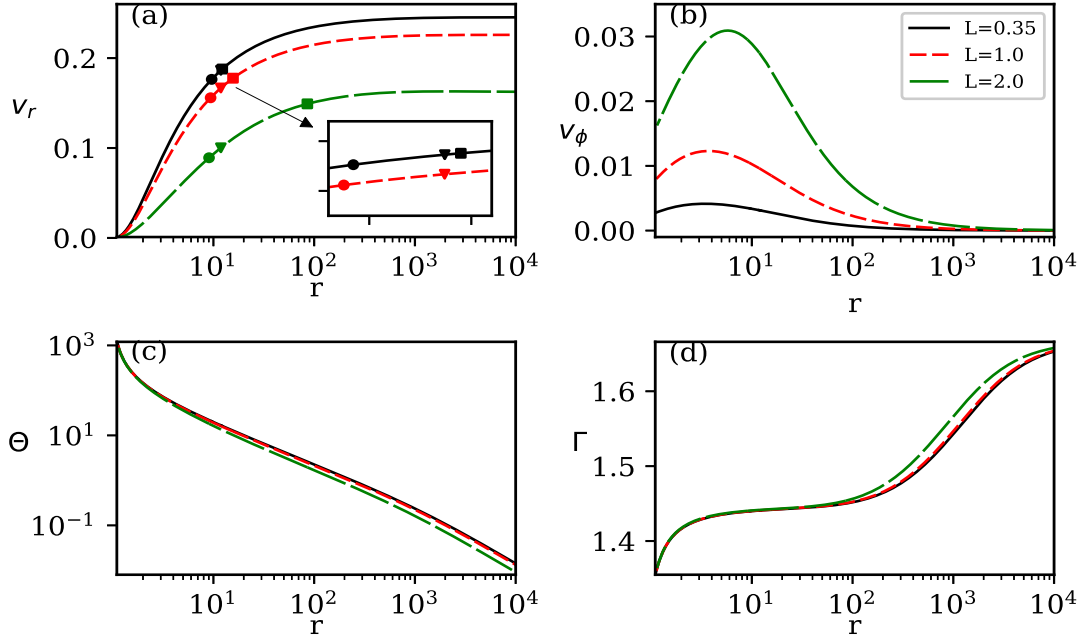


Figure 5. Flow solutions like, (a) v_r , (b) v_ϕ , (c) Θ and (d) Γ as a function of r . Each curve is for $L = 0.35$ (solid, black), $L = 1.0$ (dashed, red), $L = 2.0$ (long-dashed, green) Here $E = 1.03075$, $\xi = 1$.

(4b) we plot E_c versus $\dot{\mathcal{M}}_c$. For each value of L , all the branches for O-type and X-type critical points are present, however for low L (solid, black) the kite-tail part is very small, which implies that multiple critical points are possible only for a rotating flow. Although L has a significant effect on the parameter-space, but in order to get a more quantitative idea, one need to compare outflow solutions for different L but same E .

We compare the flow solutions, like v_r (Fig. 5a), v_ϕ (Fig. 5b), Θ (Fig. 5c) and Γ (Fig. 5d) as a function of r , for various values of $L = 0.35$ (solid, black), $L = 1.0$ (dashed, red), $L = 2.0$ (long-dashed, green). All the plots have the same Bernoulli parameter $E = 1.03075$ and $\xi = 1.0$. In Fig. (5a), the solid circle, arrow head, and square represents the positions of the slow, Alfvén and fast points, respectively. For $L = 0.35$, the Alfvén and fast points are almost merged, the inset zooms the region to resolve those two points. Outflows with higher L and same E have higher values of v_ϕ . Interestingly, outflows with higher values of L , are slower (low v_r in long-dashed curve). If one compares various terms in the equation (8), by keeping E constant but increasing L , then the budget in centrifugal and magnetic terms are larger compared to that in radial kinetic and thermal terms. Therefore, v_ϕ increases with L , but v_r and Θ decreases.

We plot the outflow streamlines in Fig. (6a) and the magnetic field lines Fig. (6b) of

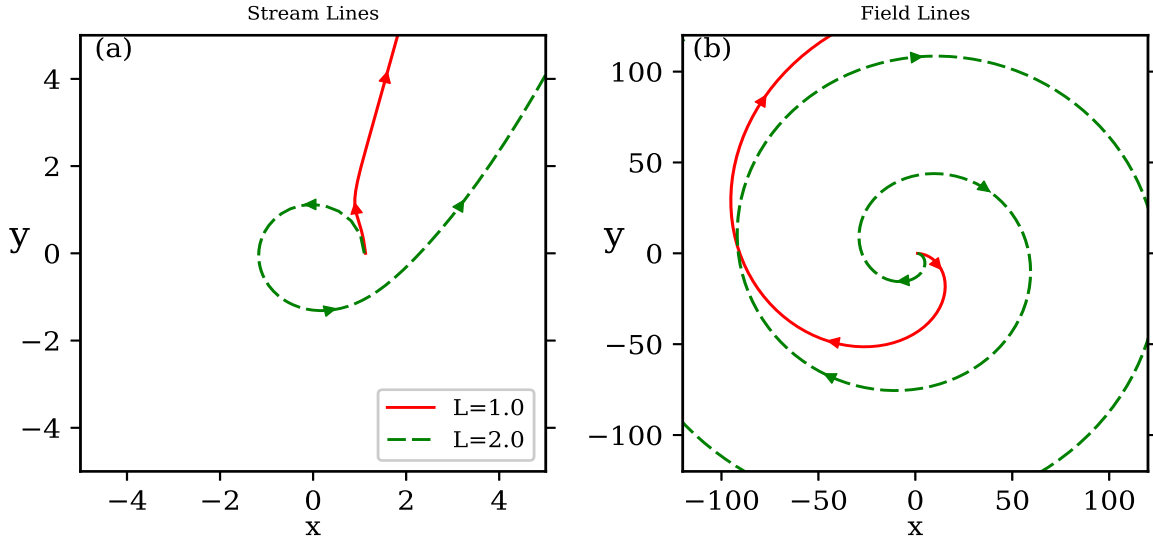


Figure 6. (a) Flow streamlines and (b) magnetic field lines. Each of the curves are for total angular momentum $L = 1.0$ (solid, red) and $L = 2.0$ (dashed, green). In both the cases $E = 1.03075$.

a plasma whose $E = 1.03075$, where total angular momenta are $L = 1.0$ (solid, red) and $L = 2.0$ (dashed, green). The wind streamline (SL) and magnetic field lines (FL) are obtained by integrating the following equations,

$$d\phi_{\text{SL}} = \frac{v_\phi}{v_r} \frac{dr}{r}; \quad \& \quad d\phi_{\text{FL}} = \frac{B_\phi}{B_r} \frac{dr}{r} \quad (21)$$

This plot reconfirms the governing equations which showed that the magnetic field is clockwise but the wind is counter clockwise. It also shows a very important effect that magnetic field has on ionized plasma. It modifies the plasma streamline by redistributing the plasma angular momentum (rv_ϕ), such that, for $L = 1.0$ flow (solid, red; Fig 6a) which was launched with a counter-clockwise rotation, is flung out even before completing a loop. So this figure presents the structure of the outflow for two angular momenta as depicted in Figs. (5). It is clear that the outflow and the magnetic field are not parallel to each other.

To study the effect of Bernoulli parameter, we compare v_r (Fig. 7a), v_ϕ (Fig. 7b), Θ (Fig. 7c) and Γ (Fig. 7d), for various values of $E = 1.01575$ (solid-black), 1.05575 (dashed-red) and 1.09975 (long-dashed-green) for a given value of $L = 1.0$. The solid circle, arrow head, and square represents the positions of the slow, Alfvén and fast points, respectively. The flow with higher E is faster (high v_r), less rotating (low v_ϕ) and hotter (high Θ) compared to

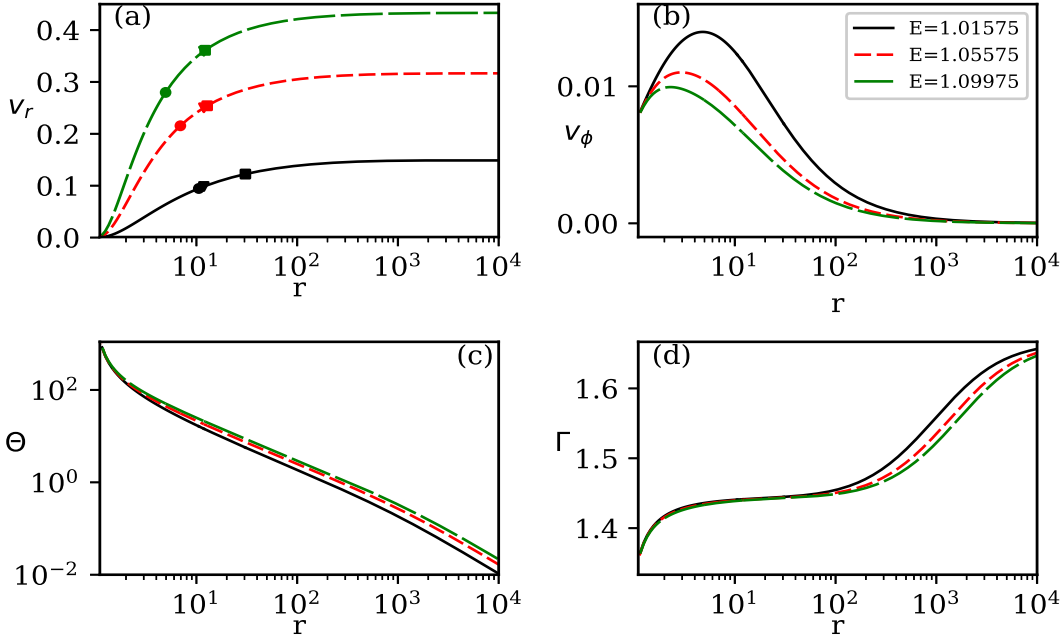


Figure 7. These are the wind solutions for different Bernoulli parameters $E = 1.01575$ (solid-black), 1.05575 (dashed-red) and 1.09975 (long-dashed-green). We have plotted the radial velocity v_r (a), v_ϕ (b), Θ (c) and Γ (d) versus radius r . All the plots are for $L = 1.0$ and $\xi = 1.0$.

flows with lower values of E . Γ is not constant in any of the cases discussed so far and it follows the Θ distribution.

In Figs. (8) we present the effect of strong gravity. We chose electron-proton or $\xi = 1.0$ plasma, where the flow has the same Bernoulli parameter E ($= 1.301$), r_A ($= 3.3859$) and total angular momentum L ($= 1.75$). However, we compare magnetized-wind solutions expanding in a region described by Newtonian gravitational potential (solid, black) with another one in a region described by PW potential (dashed, red). We chose a higher value of E , in order to maximize the effect. Even for the same specific energy and angular momentum, the wind in a region described by Φ_{PWP} is faster and hotter than the one in a region described by a Newtonian gravity. The stronger gravity of a Φ_{PWP} compresses the plasma around the compact object and produces a higher temperature flow. The inner boundary condition of the outflow in Φ_{NP} , shows that v_r (although sub-slow) is quite high, while v_ϕ and Θ is lower than that around Φ_{PWP} . The acceleration achieved for flows around Φ_{NP} is quite moderate, while that around Φ_{PWP} is significant. If we use lower E then perhaps the v_r at the inner boundary for Φ_{NP} will have proper value but then the terminal speed would be very low.

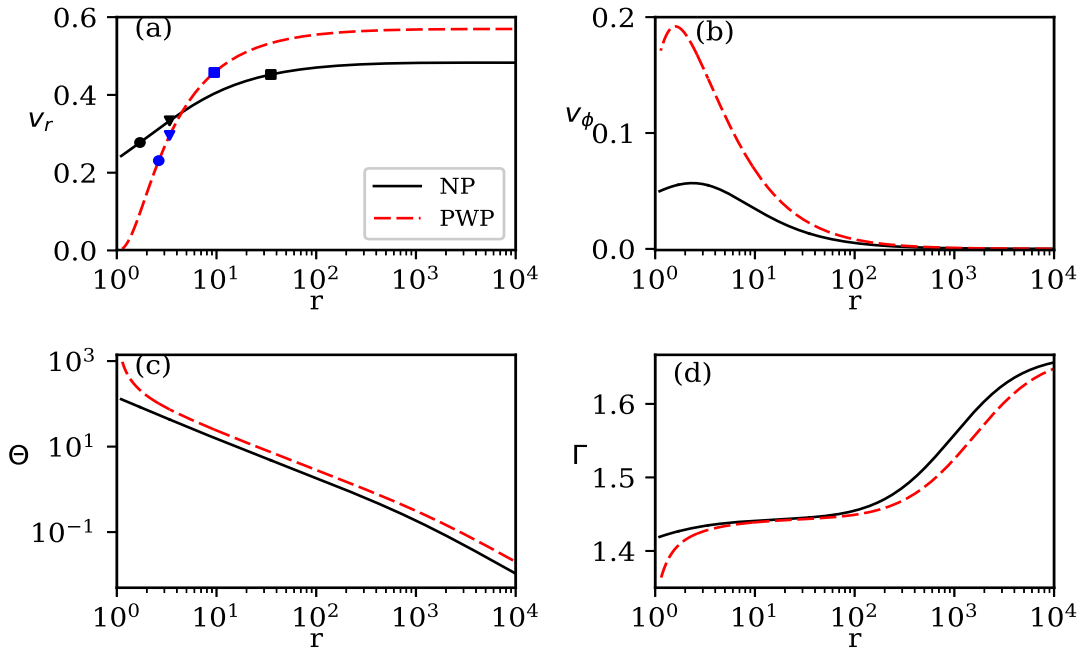


Figure 8. Wind solution in Newtonian potential Φ_{NP} (solid, black) and in Paczyński & Wiita potential Φ_{PWP} (dashed, red) for $E = 1.301$, $L = 1.75$ and $\xi = 1$. The flow variables are (a) v_r , (b) v_ϕ , (c) Θ and (d) Γ versus radius r . The slow-point, Alfvén point and fast-point are marked as solid, circle, triangle and square.

One may conclude that, if we use Φ_{NP} to describe the gravity around a compact object, then, only slow outflows can be obtained.

In Figs. (9a & b), we plot the effect of composition of the flow on its critical point properties. We plot the Bernoulli parameter as a function of critical radius i.e., E_c versus r_c , for fixed value of $L = 1.0$ and $r_A = 11.85$, but different values of composition or $\xi = 0.0$ (solid, black), $\xi = 0.5$ (dashed, red), $\xi = 1.0$ (long-dashed, green). Similar to previous E_c and $\dot{\mathcal{M}}_c$ plot, the proper wind solution corresponds to the E_c versus $\dot{\mathcal{M}}_c$ at the intersection of the X-type slow branch and X-type fast branch (marked as solid circle, triangle and a square for three values of ξ).

In Figs. (10a–d), we compare v_r , v_ϕ , Θ and Γ for flows with the same E ($= 1.03075$) and L ($= 1.0$) but for different composition $\xi = 0.05$ (solid, black), 0.5 (dashed, red) and 1.0 (long-dashed, green). All the flow variables like v_r , v_ϕ and Θ depend on ξ . The $\xi = 1.0$ or electron-proton flow has somewhat higher v_r close to the base. The lepton dominated wind ($\xi = 0.05$) has higher v_r at some intermediate range of r , but finally for a flow with a composition parameter $\xi = 0.5$, the terminal v_r or $v_r^{\text{max}} = v_r|_{r \rightarrow \infty}$ is higher than the flow with other two combinations, albeit by a small amount. This is not expected in hydrodynamics. It

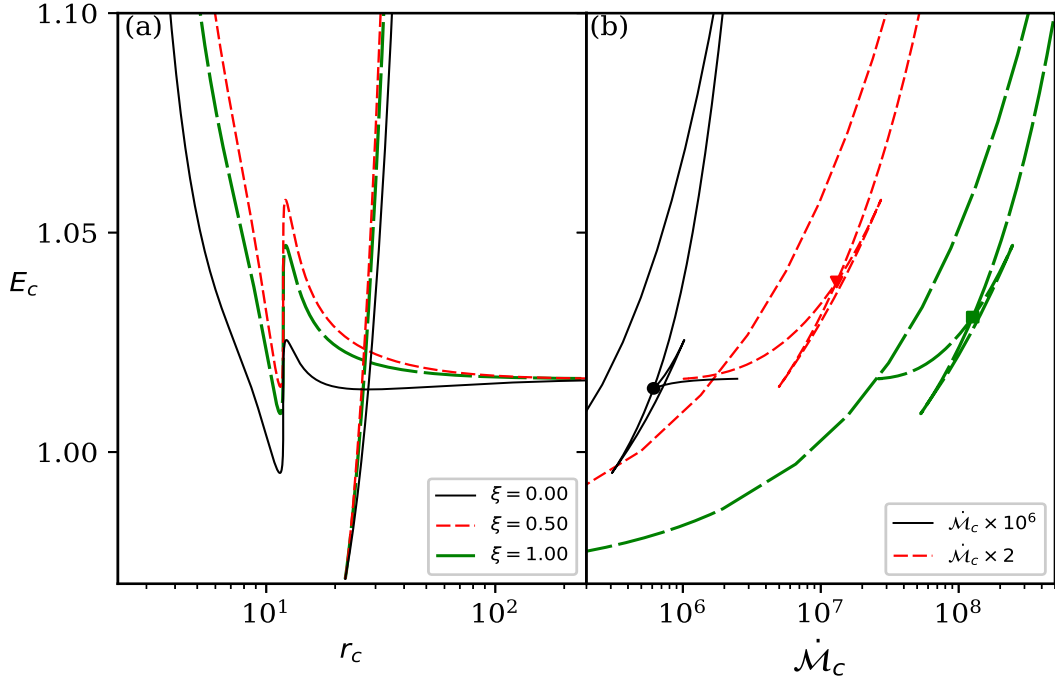


Figure 9. In panel we plot, (a) E_c versus r_c and (b) E_c versus $\dot{\mathcal{M}}_c$. The curves represent $\xi = 0.0$ (solid, black), $\xi = 0.5$ (dashed, red), $\xi = 1.0$ (long-dashed, green). All plots are for $L = 1.0$.

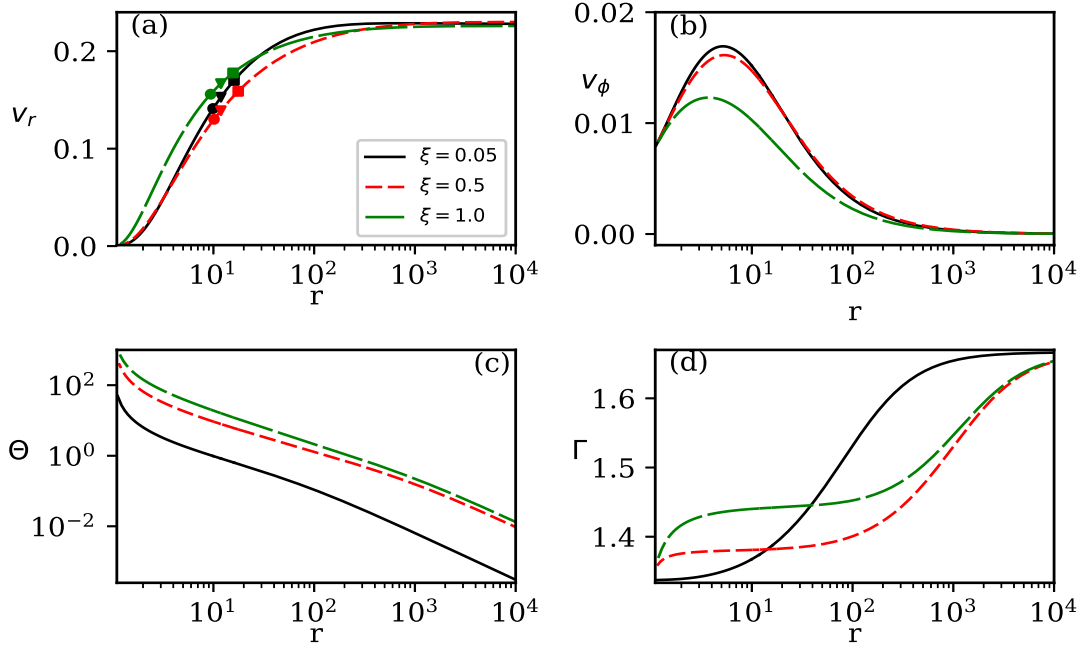


Figure 10. (a) v_r , (b) v_ϕ , (c) Θ and (d) Γ as a function of r , where each curve represent $\xi = 0.05$ (solid, black), $\xi = 0.5$ (dashed, red) and $\xi = 1.0$ (long-dashed, green). All the curves have the same $E = 1.03075$ and $L = 1.0$.

may be noted that, in hydrodynamics for $r \rightarrow$ large, $h \rightarrow 1$, centrifugal term $\rightarrow 0$, $\Phi(r) \rightarrow 0$, $v_r^{\max} \rightarrow \sqrt{2(E-1)}$. In other words, the terminal speeds of winds in hydrodynamics do not depend on composition, but for MHD winds, even as $r \rightarrow$ large, $h \gtrsim 1$ because of the presence of the magnetic term and hence v_r^{\max} depends on ξ . The azimuthal velocity v_ϕ also depends on ξ , where an electron-proton flow has the least v_ϕ distribution when compared with flows of higher proportion of leptons. However, $v_\phi \rightarrow 0$ at $r \rightarrow$ large, therefore the asymptotic value of v_ϕ does not depend on ξ . It may be noted that, the effect of ξ cannot be studied by attributing some scale factor, as one can clearly see that, the v_ϕ curves intersect for flows with $\xi = 0.5$ and 0.05 . Similar to all the studies in the hydrodynamic regime in the present case too, the temperature distribution $\Theta(r)$ is highest for $\xi = 1.0$. Although Θ is high for $\xi = 1.0$ compared to other flows with $\xi < 1$, the Γ for electron-proton flow is not the lowest. In fact, at lower values of r , $\Gamma_{\xi=0.05} < \Gamma_{\xi=0.5} < \Gamma_{\xi=1}$. This is because, Γ compares the thermal energy of the plasma compared to its inertia, hence high value of Θ cannot compensate for higher inertia of an electron-proton flow. In comparison, a lepton dominate flow ($\xi = 0.05$) achieves $\Gamma \rightarrow 4/3$, in spite of starting with a temperature at least an order of magnitude less than that of an electron-proton flow.

In Figs. (11) we have plotted v_r^{\max} as a function of ξ , for various values of energies ($E = 1.15475, 1.04575, 1.03075, \text{ and } 1.01075$) and a given value of L . It is interesting to note that terminal speed distribution for higher to lower energies of the magnetized outflow, depends on ξ . For higher energies, it decreases with ξ , but for lower E , v_r^{\max} maximizes at some value of ξ . The maxima depends on E . This is a significantly different result compared to hydrodynamics. This effect arises due to the competition between pressure gradient and magnetic forces in the equations of motion.

5 DISCUSSION AND CONCLUSIONS

Our main focus is on studying the effect of variable Γ EoS and the composition on magnetized wind solutions. This model is the bedrock over which magnetized jet models were developed later. In this context, it may be noted that there are of course many models of generation of outflows around compact objects, tailored to address different scenarios. For example, if the underlying accretion disc is luminous then radiation can drive outflows via scattering processes (Icke 1980; Tajima & Fukue 1996, 1998; Moller & Sadowski 2015; Yang et. al. 2018; Vyas & Chattopadhyay 2019) or for cooler gases via the line driven processes (Nomura et. al.

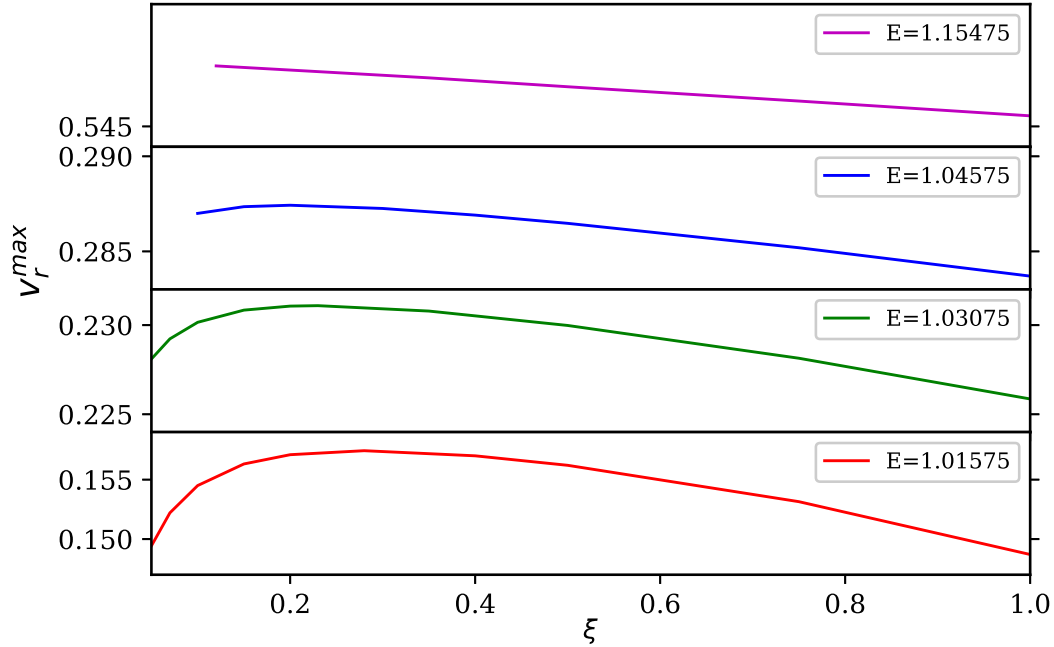


Figure 11. Terminal speed v_r^{\max} is plotted as a function of ξ from top panel and downwards for $E = 1.15475, 1.04575, 1.03075,$ and $1.01075,$ respectively. $L = 1.0$ for all the curves.

2016; Nomura & Ohsuga 2017). In case the accretion flow is low luminous flow then magnetic, gas pressure and centrifugal term may drive outflows (Gu 2015; Yuan et. al. 2015; Bu et. al. 2016a,b; Bu & Mosallanezhad 2018). In the present paper we are also working in the regime where radiation is not important. However, our main focus is to study a typical transmagnetosonic outflow solution and what are the parameters these solutions depend on. In particular, the effect of a variable Γ EoS and different composition of the plasma on the outflow solution has probably not been studied before.

In this paper we have revisited magnetized, wind model using Paczyński & Wiita potential, variable Γ EoS and for various values of total angular momentum (L), Bernoulli parameter (E) and composition (ξ) of the flow. E and L are constants of motion. However, as is the case in hydrodynamics, in MHD too, there can be a plethora of solutions corresponding to the same set of constants of motion. As has been shown by Bondi (1952), of all the possible solutions related to a given set of constants of motion, the physical global solution is the one which has the highest entropy and also happens to be the transonic one. Similarly in MHD (Figs. 2), it was shown that the solution passing through slow, Alfvén and fast points is the correct solution. We have found that for a given set of values of E and ξ , higher angular momentum outflows are slower (lesser v_r) compared to flows with lower L .

This is understandable, since matter which is rotating faster, will not be able to possess higher v_r . In particular, for flows with lower L , magnetic field may deflect outflow from counter clockwise to a quasi-radial flow relatively close to the central object (Fig. 6a). In other words the effect of magnetic field cannot be quantified by how much the flow is accelerated radially, but magnetic field has a very important role in regulating flow angular momentum. We also show that faster outflow is possible, for flows with higher E . Interestingly, the Θ differs slightly if E or L is changed, but the change in v_r and v_ϕ is more significant. However, v_r , v_ϕ and Θ distributions are significantly different for different values of ξ . This is because, if we change the composition of the flow, then we are not only changing its thermal energy content (which pushes the matter outward), but also inertia of flow. Therefore, the terminal speed of the outflows at a given value of E and L maximizes at a given value of ξ . Although, the ξ at which the peak of v_r^{\max} will occur, also depends on E . The peak steadily shifts to higher ξ as E decreases. Dependence of various flow variables on ξ for MHD flows probably has not been reported before. In addition, the spectra emitted by such winds should be quite different for different values of ξ , since the different velocity distributions would result in different density distributions. Moreover, different temperature distributions would strongly determine the processes that would dominate the emission. We also studied the wind solutions in different gravitational potentials to show how the compactness of central object affect the outflow solutions.

APPENDIX A: COMBINATION OF FORCES FOR MAGNETIZED OUTFLOW

Here we plot the competing combined forces acting on a magnetized wind/outflow. The thermal force is F_T , rotational force is F_R , F_G is the gravitational and F_M is the magnetic force along the stream line, as is described in connection with Figs. (3d). We plot $F_T + F_G$ (solid, black) and $F_R + F_M$ (dashed, red) in Fig. A1 in order to compare the competing forces. Clearly $F_R + F_M$ is comparable $F_T + F_G$ close to the central object where it is launched, but is larger at very large distances. However, $F_T + F_G$ dominates over the other combination very close to the central object till unto a hundred r_g .

REFERENCES

Bondi H., 1952, MNRAS, 112, 195

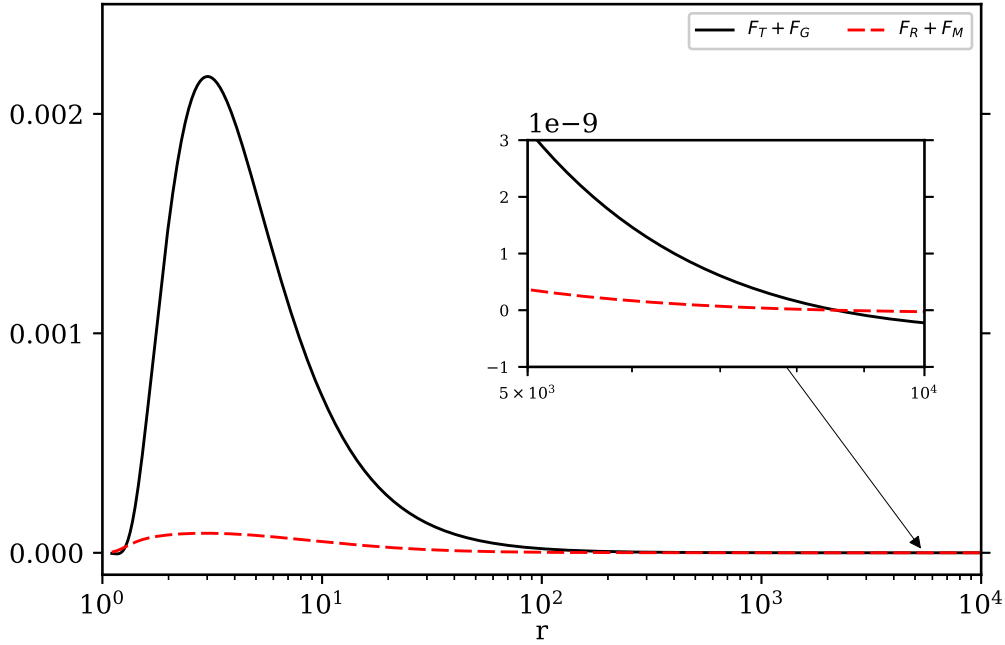


Figure A1. Comparison of combination of forces thermal and gravitational $F_T + F_G$ (solid, black) and rotational and magnetic forces $F_R + F_M$ (dashed, red) along the streamline. The flow parameters are $E = 1.03075$, $L = 1.0$ and $\xi = 1.0$ same as Fig. 3.

Blandford R. D., Payne D. G., 1982, MNRAS, 199, 883.

Bu De-Fu, et. al., 2016a, ApJ, 818, 83

Bu De-Fu, et. al., 2016b, ApJ, 823, 90

Bu De-Fu, Mosallanezhad A., 2018, A&A, 615, A35

Camenzind M., 1986, A&A, 156, 137.

Chandrasekhar S., 1938, An Introduction to the Study of Stellar Structure (NewYork, Dover).

Chattopadhyay, I., Ryu D., 2009, ApJ, 694, 492.

Chattopadhyay I., Kumar R., 2016, MNRAS, 459, 3792

Daigne F., Drenkhahn G., 2002, A&A, 381, 1066

Gu Wei-Min, 2015, ApJ, 799, 71

Heinemann M., Olbert, S., 1978, J. Geophys. Res., 83, 2457.

Icke V., 1980, AJ, 85, 239

Kumar R., Singh C. B., Chattopadhyay I. Chakrabarti S. K., 2013, MNRAS, 436, 2864.

Kumar R., Chattopadhyay I., 2014, MNRAS, 443, 3444.

Kumar R., Chattopadhyay I., 2017, MNRAS, 469, 4221.

Lovelace R. V. E., Berk H. L., Contopoulos J., 1991, ApJ, 379, 696.

- Lovelace R. V. E., Romanova M. M., Bisnovaty-Kogan G. S., 1995, MNRAS, 275, 244
- Mestel L., 1967, Plasma Astrophysics, ed. Sturrock, P. A., Academic Press, New York.
- Mestel L., 1968, MNRAS, 138, 359.
- Moller A., Sadowski A., 2015, arXiv 1509.06644
- Nomura M., Ohsuga K., Takahashi H. R., Wada K., Yoshida T., 2016, PASJ, 68, 16
- Nomura M., Ohsuga K., 2017, MNRAS, 465, 2873
- Okamoto I., 1974, MNRAS, 166, 683.
- Okamoto I., 1975, MNRAS, 173, 357.
- Paczynski B., Wiita P. J., 1980, A&A, 88, 23.
- Polko P., Meir D. L., Markoff S., 2010, ApJ, 723, 1343
- Pneuman G. W. & Kopp, R. A., 1971, Sol. Phys., 18, 258.
- Sakurai T. 1985, A&A, 152, 121.
- Sakurai T. 1987, PASJ, 39, 821.
- Singh K., Chattopadhyay I., 2018, MNRAS, 476, 4123.
- Tajima Y., Fukue J., 1996, PASJ, 48, 529
- Tajima Y., Fukue J., 1998, PASJ, 50, 483
- Vyas M. K., Kumar R., Mandal S., Chattopadhyay I., 2015, MNRAS, 453, 2992.
- Vyas M. K., Chattopadhyay I., 2017, MNRAS, 469, 3270.
- Vyas M. K., Chattopadhyay I., 2018, A&A, 614, A51
- Vyas M. K., Chattopadhyay I., 2019, MNRAS, 482, 4203
- Weber E. J., Davis L., Jr., 1967, Astrophysical Journal, 148, 217.
- Yang X.-H., Bu D.-F., Li Q.-X., 2018, ApJ, 867, 100
- Yuan F., et. al., 2015, ApJ, 804, 101.